

Can Near-Critical Solvents Drive Colloidal Self-Assembly?

John R. Edison,¹ Nikos Tasios,¹ Simone Belli,² Robert Evans,³ René van Roij,² and Marjolein Dijkstra^{1,*}

¹*Soft Condensed Matter, Utrecht University, Princetonplein 5, 3584 CC Utrecht, The Netherlands*

²*Institute for Theoretical Physics, Utrecht University,
Leuvenlaan 4, 3584 CE Utrecht, The Netherlands*

³*H.H. Wills Physics Laboratory, University of Bristol, Bristol BS8 1TL, United Kingdom*

In 1978 Fisher and de Gennes predicted the existence of long-ranged solvent-mediated (SM) interactions between two colloidal particles suspended in a near-critical binary solvent. The range of these (universal) SM forces, often referred to as critical Casimir forces, is set by the correlation length of the solvent which diverges on approaching its critical point. The remarkable sensitivity of SM interactions to the temperature and composition of the solvent sparked recent interest, driven by prospects of unparalleled control of colloidal self-assembly in a tunable, reversible, and in-situ fashion. Here we determine both the effective SM pair interactions and the *full* phase diagram of Brownian discs suspended in an explicit two-dimensional *supercritical* binary liquid mixture. The SM pair interactions are most attractive at off-critical compositions of the solvent, and combined with the SM many-body interactions they drive colloidal gas-liquid and fluid-solid phase transitions in a surprisingly large regime *away* from criticality. Our simulation study, supported by a mean-field theory, provides a fresh perspective on colloidal self-assembly mediated by solvent critical fluctuations, and opens new avenues for controlling and manipulating this process.

Colloidal particles dispersed in a binary solvent mixture have an inherent preference for one of the two sol-

vent species. This is reflected by preferential adsorption of the favoured species on the colloid surface, under suitable thermodynamic conditions. The adsorbed films mediate an effective interaction between two colloidal particles which is remarkably sensitive to the thermodynamic state of the solvent. Close to the (demixing) critical point of the solvent the adsorbed film thickness is determined by the correlation length ξ of the solvent [1] and, as first predicted by Fisher and de Gennes [2], the resulting solvent-mediated (SM) interactions are long ranged with universal scaling properties. An analogy between the confinement of quantum fluctuations of the electromagnetic field [3] and that of thermal composition fluctuations in a near-critical binary solvent led to these (universal) SM forces being referred to as critical Casimir forces.

Theoretical studies on near-critical fluids confined between a pair of infinitely large planar walls (representing two static large colloids) [4–8], along with direct experimental measurements of the Casimir force [9, 10] have advanced our understanding of the nature of two-body SM interactions. However, the phase behaviour of a *dense* suspension of *Brownian* colloids of *finite* size is largely unexplored, due to the geometrical complexity and the high dimensional parameter space; these demand massive computational costs. Here we seek to understand the strength and range of the SM interactions and the resulting self-assembled structures in a dense colloidal suspension as a function of the thermodynamic state of the solvent via computer simulations. The conventional approach of treating the solvent implicitly via an effective two-body colloidal pair interaction is likely to fail as the SM interactions are expected to be highly non-additive [11]. On the other hand, computer simulation of colloids in an explicit molecular solvent with a bulk correlation length that diverges upon approaching the critical point is notoriously difficult as very different length and time scales are involved. Nevertheless, by sacrificing one spatial dimension and using a lattice model, we have been able to calculate the SM interactions and *full* phase diagrams for a ternary solvent-solvent-colloid mixture, thereby revealing phenomena not captured by treatments based *solely* on effective pair potentials extracted from the *static* planar slit system [12].

We model the ternary solvent-solvent-colloid mixture as an incompressible ABC mixture on a 2D square lattice, as shown schematically in Fig. 1. Colloids C are

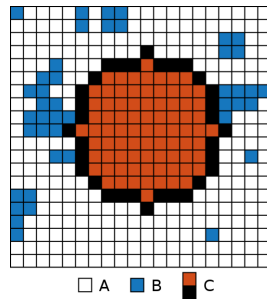


FIG. 1. A schematic representation of the solvent-solvent-colloid lattice model. White cells are occupied by solvent species A, blue cells by solvent species B, and brown and black cells represent the interior and the boundary of a single colloidal particle C, respectively. Nearest neighbour AB pairs experience a repulsive potential $\epsilon/2$, and nearest neighbour BC pairs an attractive potential $-\alpha\epsilon/2$.

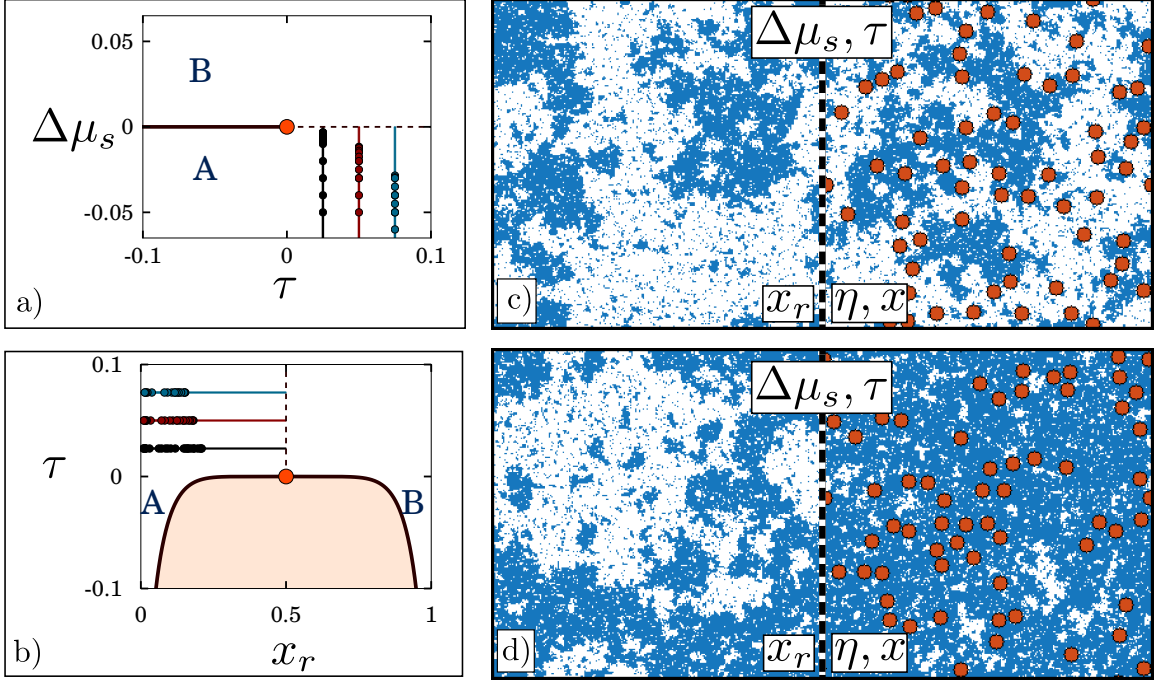


FIG. 2. **Ternary ABC solvent-solvent-colloid mixture** : a) Phase diagram (binodal) of the colloid-free AB solvent mixture plotted as $\Delta\mu_s$ vs τ . b) Phase diagram (binodal) of the same mixture plotted as τ vs x_r , the composition of the solvent. The two coexisting phases for $\tau < 0$ are designated A and B. In a) and b) the lines correspond to the paths along which the phase diagram of the full ternary ABC mixture is determined; the dots represent the states where phase coexistence is observed and the orange dot indicates the critical point of the AB solvent mixture $\{\tau = 0, \Delta\mu_s = 0\}$. c) Typical configurations of a ternary ABC mixture (right) with neutral colloids with no preference for A or B (radius $R = 6$, $\alpha = 0$) at colloid packing fraction $\eta = 0.11$ and solvent composition $x = (1 - \eta)/2$ in equilibrium with a solvent reservoir (left) with $\eta = 0$, $x_r = 1/2$, $\tau = 0.005$, and bulk correlation length $\xi \approx 19R$. d) Typical configurations of a ternary ABC mixture (right) with colloids strongly preferring solvent B ($R = 6$, $\alpha = 19.0$) at packing fraction $\eta = 0.11$ and solvent composition $x > (1 - \eta)/2$ in equilibrium with the same solvent reservoir (left) as in (c).

discretized hard discs with a radius of R lattice sites, occupying a fraction η of the lattice sites. Every site that is left unoccupied by the colloidal discs is occupied by either a solvent molecule of species A or B, such that the fraction of sites occupied by A and B equals $1 - \eta - x$ and x , respectively. We consider only nearest neighbour AB repulsions and BC attractions: an energy penalty $\frac{1}{2}\epsilon > 0$ is assigned to every nearest neighbour AB pair to drive AB demixing at sufficiently low temperatures T , and an energy gain $-\frac{1}{2}\alpha\epsilon$ with $\alpha \geq 0$ for every BC pair to mimic the colloid C's preference for species B. Throughout we set the lattice spacing to unity.

In the limit $\eta = 0$, our model reduces to a binary AB mixture that is isomorphic to the 2D lattice (Ising) model, the workhorse in studies on critical phenomena and inhomogeneous fluids for the last four decades. The critical temperature of this binary mixture is $T_c = 0.567\epsilon/k_B$, and its thermodynamic state is characterized fully by the reduced temperature $\tau = (T - T_c)/T_c$ together with either the reduced chemical potential difference $\Delta\mu_s = (\mu_B - \mu_A)/\epsilon$ between species B and A or the composition x . For $\Delta\mu_s < 0$ the AB mixture favours an A-rich composition at all temperatures. More-

over for $\tau < 0$ demixing into an A-rich state ($x < 0.5$) and a B-rich state ($x > 0.5$) takes place at $\Delta\mu_s = 0$, with a critical point $\{\tau_c = 0, x_c = 0.5\}$, see Fig. 2a and b. In the two limits $\Delta\mu_s \rightarrow \pm\infty$ our ABC mixture reduces to the 2D AC or BC hard-disc system with packing fraction η in an (irrelevant) pure A solvent ($x = 0$) or pure B solvent ($x = 1 - \eta$). Barring small discretization and lattice artifacts, and ignoring subtleties regarding the (non-)existence of a stable hexatic phase, these AC and BC systems exhibit fluid-solid coexistence for $\eta \in [0.700, 0.716]$ as represented by vertical dashed lines in Fig. 3a-c [13].

Throughout this work we study colloids immersed in a *supercritical* (one-phase) AB mixture, relatively poor in the colloid-preferred species B ($\eta > 0$, $\tau > 0$, and $\Delta\mu_s \leq 0$). This choice precludes solvent-mediated colloidal aggregation arising from complete wetting and capillary condensation [14]. We consider first the case of neutral colloids which have no preference for species A or B ($R = 6$, $\alpha = 0$) [15]. The solvent is treated grand canonically, i.e. we fix $\Delta\mu_s$ and τ , and thus the composition x_r of the reservoir, and we consider a colloidal suspension at given η in osmotic equilibrium with this

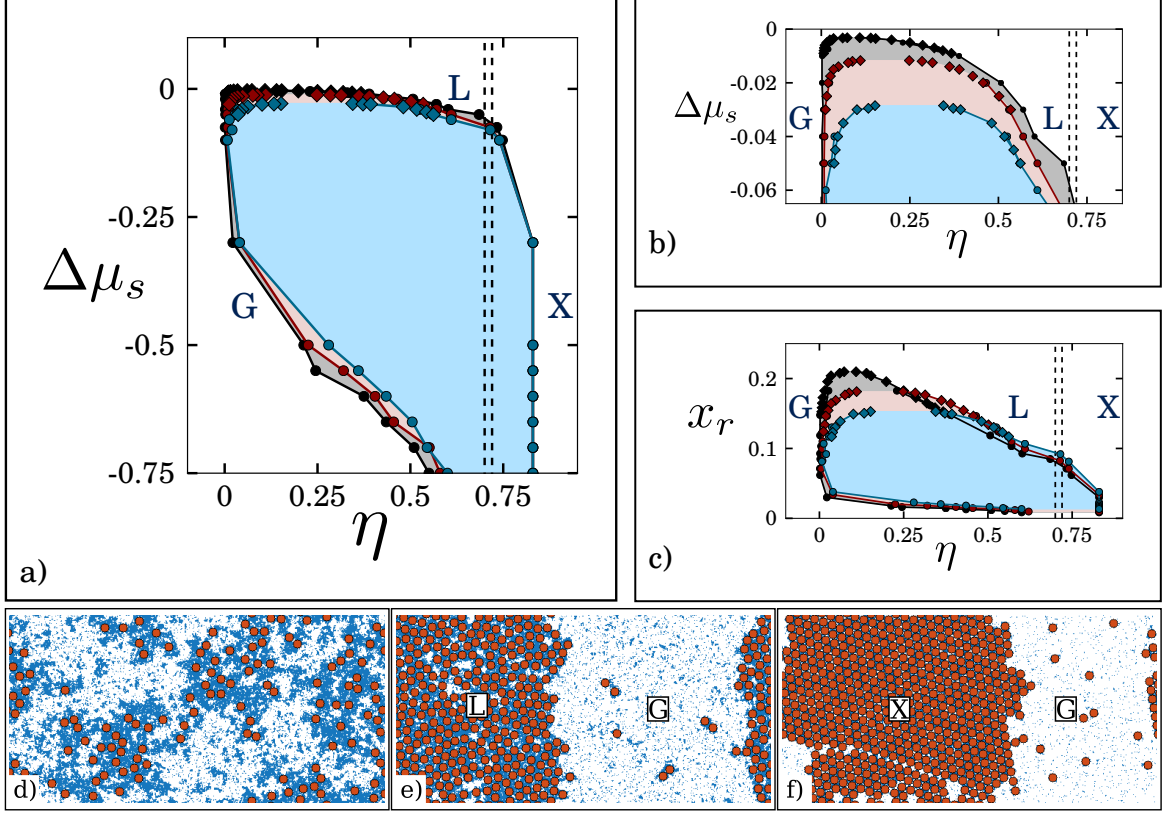


FIG. 3. **Phase diagrams and typical snapshots** : a) Phase diagrams of the full ABC ternary mixture plotted as solvent chemical potential $\Delta\mu_s$ vs hard disc (colloid) packing fraction η for $R = 6$. b) The top portion of a) is replotted for clarity. c) Phase diagram of the ABC model plotted as reservoir solvent composition x_r vs η . Black, red and blue symbols refer to $\tau = 0.025, 0.05$ and 0.075 . The diamonds and dots denote the phase boundaries obtained from grand canonical staged insertion Monte Carlo (MC) simulations and canonical ensemble MC simulations, respectively (see Methods). The vertical dashed lines denote fluid-solid coexistence for pure hard discs. d - f) Simulation snapshots of a system of 256×512 lattice sites at $\tau = 0.05$ and $\alpha = 0.6$, showing d) a supercritical colloidal phase at $\Delta\mu_s = -0.005$ of 128 colloids, e) gas-liquid (G-L) coexistence at $\Delta\mu_s = -0.04$ of 348 colloids, and f) gas-crystal (G-X) coexistence at $\Delta\mu_s = -0.3$ of 580 colloids.

reservoir. The ABC mixture has composition $x \neq x_r$. This is illustrated in Fig. 2c where we show a snapshot of a system of neutral colloids (right) at $\tau = 0.005$ and $\Delta\mu_s = 0$ in equilibrium with the solvent reservoir (left). The snapshots reveal the tendency of the colloids to preferentially adsorb at the ‘interfaces’ between the instantaneous (*supercritical*) A and B domains. This feature, which resembles the binding of colloids to static air-liquid or liquid-liquid interfaces by a Pieranski potential [16], is captured here owing to the finite size and the Brownian character of the colloids. Fig. 2d shows snapshots for the same parameter set, except now the colloids strongly prefer solvent B ($\alpha = 19$). The strong B-adsorption on the colloids and the unfavourable AB interaction lead to an overall excess of B, thereby driving the ABC mixture far away from criticality; the solvent correlation length is clearly observed to be far below the particle size.

In the remainder of this study we focus on the case $\alpha =$

0.6 where B-rich layers adsorbed on the colloid surfaces compete with a supercritical A-rich bulk solvent ($\tau > 0$ and $\Delta\mu_s < 0$). In Figs. 3a and b we present the phase diagram of the full ternary ABC mixture in the $\Delta\mu_s$ vs η representation at three reduced temperatures $\tau = 0.025, 0.05, 0.075$. The correlation length of the AB solvent at the isochoric composition ($\Delta\mu_s = 0, x_r = 0.5$) is given by $\xi = 0.567/\tau$, and for these temperatures: $\xi_{0.025} = 22.68$, $\xi_{0.05} = 11.35$, $\xi_{0.075} = 7.56$, which are of the same order as the size of the colloid $R = 6$. Although the underlying AB solvent mixture is supercritical our simulations reveal that a non-zero concentration of large Brownian discs induces stable colloidal gas (G), liquid (L), and crystal (X) phases as well as two-phase G-L and G-X coexistence. The G-L coexistence, which is shown more clearly in Fig. 3b, terminates at a critical point that shifts to lower $\Delta\mu_s$ and higher η with increasing τ . For $\Delta\mu_s < -0.1$ we also observe G-X coexistence

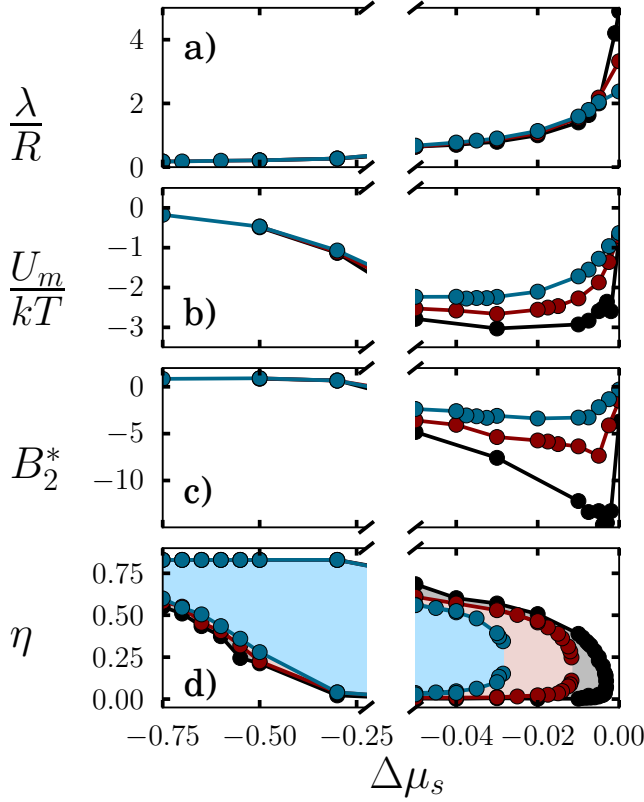


FIG. 4. **Effective two-body SM interactions** a) Thickness λ of the B-rich film adsorbed on a single hard disc, b) The minimum well depth of the effective two-body SM potential, c) The reduced second virial coefficient B_2^* , d) The phase boundaries of the ternary ABC mixture plotted as hard disc packing fraction η vs $\Delta\mu_s$. Black, red and blue symbols refer to reduced temperatures $\tau = 0.025, 0.05$ and 0.075 respectively ($R = 6, \alpha = 0.6$).

with a broad colloid density gap that narrows sharply upon lowering $\Delta\mu_s$, consistent with the limiting hard-disc fluid-solid coexistence at $\Delta\mu_s \rightarrow -\infty$ (vertical dashed lines). Significantly, this decreasing density gap at G-X coexistence suggests an additional underlying metastable G-L lower critical point. Although we have not been able to identify this in our MC simulations, it does occur in our mean-field theory presented below. Moreover, if we accept hard-disc coexistence in the opposite limit $\Delta\mu_s \rightarrow \infty$, then we also expect a G-L-X triple point at $\Delta\mu_s \simeq -0.06$ for $\tau = 0.025$ (see Fig. 3b), and at even lower $\Delta\mu_s$ for higher τ .

In Figs. 3d - 3f we show typical snapshots of systems of 256×512 lattice sites simulated at reduced temperature $\tau = 0.05$ ($\alpha = 0.6, R = 6$). These illustrate configurations of (d) supercritical (homogeneous single-phase) fluid state, (e) G-L coexistence, and (f) G-X coexistence. It is clear that in all three cases the local solvent composition is strongly correlated with the local colloid density, such that the coexisting L phase in (e) and X phase in (f) essentially have a binary BC composition with tiny

traces of A. Conversely in the coexisting G phases shown in Figs. 3e and 3f the solvent composition is very close to the composition of the reservoir $x \simeq x_r$. In Fig. 3c we convert the phase diagrams of both Fig. 3a and 3b into the $x_r - \eta$ representation. It is evident from the snapshots and Figs. 3c and 2b that for all observed G-L and G-X coexistence: (i) the composition of the solvent reservoir $x_r < 0.2$, is far from the critical composition of the pure solvent $x_c = 0.5$, and (ii) the correlation length of the solvent is much smaller than the colloid radius, $\xi < R$. Strikingly, in the homogeneous supercritical state of Fig. 3d the correlation length (the typical size of the A-rich and B-C-rich “patches”) is clearly much larger than the colloid radius and thus far exceeds that of the solvent reservoir. This reflects the nearby critical point of the colloidal G-L transition, which appears to be continuously connected to the critical point of the binary AB solvent mixture (at $\eta = \tau = \Delta\mu_s = 0$). Accurate estimates of the critical points for $\tau < 0.025$ are prohibited by limited computational resources.

In order to understand further the genesis of the observed phase behaviour, we calculated several one- and two-colloid properties for the range of thermodynamic states studied above. For the three temperatures investigated we show in Fig. 4 the dependence on $\Delta\mu_s$ of (a) the thickness λ of the adsorbed B-rich film onto a single disc, (b) the minimum U_{min} of the effective pair potential $U(r) = -k_B T \log[P(r)/P(\infty)]$, defined in terms of the probability distribution $P(r)$ to find two colloids separated at a center-of-mass distance r , as obtained from the transition matrix Monte Carlo method, and (c) the reduced second virial coefficient $B_2^* = \int_0^\infty (1 - \exp[-U(r)/k_B T]) r dr / 2R^2$, which is normalized to that of 2D hard discs. For comparison, we also show in Fig. 4d the phase diagrams in the $\eta - \Delta\mu_s$ representation. The film thickness λ and the well depth U_{min} are measures of the range and strength of $U(r)$, respectively. The quantity B_2^* is a well-established (dimensionless) measure of combined strength and range that must be sufficiently negative in order for gas-to-liquid condensation to occur in systems described by pairwise additive interactions. Fig. 4a shows a monotonic increase of the film thickness from $\lambda \ll R$ to $\lambda \gg R$ as the isochoric composition is approached ($\Delta\mu_s \rightarrow 0$). In the same range the strength U_{min} varies non-monotonically being strongest at slightly negative $\Delta\mu_s$, reaffirming earlier theoretical predictions [17, 18]. Although $U(r)$ is long-ranged at $\Delta\mu_s \simeq 0$ it is *not* sufficiently attractive to drive G-L coexistence - see the phase diagram in Fig. 3b and 4d. Upon further decreasing $\Delta\mu_s$, however, $U(r)$ does become sufficiently attractive for colloidal G-L and G-X coexistence to occur even though the adsorbed film thickness λ (and thereby the range of $U(r)$) decreases. This is also reflected by the non-monotonic behaviour of B_2^* . Interestingly, upon lowering $\Delta\mu_s$ further the broad G-X coexistence remains whereas the range and the strength of $U(r)$ are so small

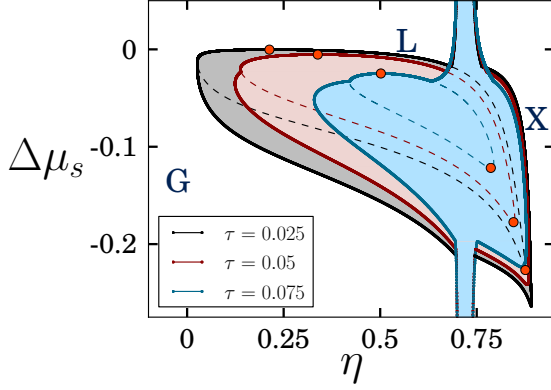


FIG. 5. **Mean-Field predictions for the Phase diagrams:** Binodals (full lines) of the colloid solvent system as calculated within mean field theory for the reduced temperatures $\tau = 0.025$ (black), $\tau = 0.05$ (red), and $\tau = 0.075$ (blue). For each τ the upper and lower (G-L) critical points are indicated by the orange dots. The dashed lines correspond to the metastable colloidal gas-liquid coexistence.

and weak, respectively, that B_2^* increases and even becomes positive. In other words, in this regime the phase diagram of the full ABC mixture reflects the importance of non-pairwise effective SM interactions. Our simulation results clearly indicate that the usual paradigm of employing only effective pair potentials as obtained from e.g. planar slit studies and the Derjaguin approximation simply breaks down when it comes to describing the full phase diagram of the ternary mixture.

In analogy with colloid-polymer mixtures, the narrowing of the G-X phase boundaries (see Fig. 3a) and the short range of the SM interactions (see Fig. 4a), upon lowering $\Delta\mu_s$, strongly suggests the existence of an underlying metastable G-L critical point. Within a mean-field approximation we analyzed the Helmholtz free energy associated with the Hamiltonian of our ABC model. In Fig. 5, we plot the resulting phase diagrams for various $\tau > 0$, which reveal a closed-loop immiscibility gap and *two* G-L critical points. The upper critical point approaches smoothly the critical point of the colloid-free AB solvent mixture as $\tau \rightarrow 0$. Interestingly, we find that the immiscibility gap shrinks with increasing τ until the two critical points merge and disappear at $\tau \simeq 0.1$. We also observe coexistence of two crystal phases with the same symmetry but different lattice spacings, also terminating at a critical point. The *topology* of the mean-field phase diagram and its τ -dependence are remarkably consistent with that obtained from simulations.

Our findings reveal that the topology of the phase diagram of colloidal particles in a near-critical binary solvent stems from an intricate balance between competing colloid-solvent and solvent-solvent couplings that can only be captured in a treatment of the full ternary mixture. The picture that emerges is that the resulting

many-body SM interactions between the colloids will drive colloidal G-L and G-X phase transitions with a strong accompanying solvent demixing, but only when the solvent correlation length is of the order of the colloidal size or smaller. Although our results are for a 2D model the resulting phase behavior is likely to pertain in 3D for hard-sphere like colloids. Thus our results also question the notion that universal *pairwise critical* Casimir forces can account for the mechanism behind colloidal aggregation reported in recent experimental work [19, 20]. Our study opens new avenues for reversibly manipulating and controlling self-assembly processes of e.g. cellular membrane proteins [21] and colloidal nanoparticles in solvent mixtures.

Methods Summary

Model and simulations

Our model is based on those of Rabani *et al.* [22]. We model the ternary solvent-solvent-colloid mixture as an incompressible ABC mixture on a 2D square lattice. Colloids C are discretized hard discs (HD) with a radius of R lattice sites that can undergo translational motion on the square lattice. The hard-disc Hamiltonian H_C is zero for non-overlapping configurations, and infinity if any pair of colloids overlap. Every lattice site i has an occupancy number $n_i = 1$ if it is occupied by a colloidal disc, and 0 if it is available for an A or a B solvent molecule with occupancy number $s_i = -1$ if it is occupied by A, and $s_i = 1$ for B. We consider only nearest neighbour interactions, and assign an energy penalty $\epsilon/2 > 0$ for every nearest neighbour AB pair to drive AB demixing at sufficiently low temperatures, and an energy gain of $-\alpha\epsilon/2$ with $\alpha \geq 0$ for every BC pair to mimic preferential adsorption of solvent B on the colloid surfaces. The total Hamiltonian thus reads

$$H = H_C + \frac{\epsilon}{4} \sum_{\langle i,j \rangle} (1-s_i s_j)(1-n_i)(1-n_j) - \frac{\alpha\epsilon}{4} \sum_{\langle i,j \rangle} n_i(1+s_j)(1-n_j) \quad (1)$$

where the summation runs over the set of distinct nearest neighbour pairs ij . We performed simulations in an elongated simulation box of 256×512 sites for three different values of the reduced temperature $\tau = 0.025, 0.05$, and 0.075 . At each τ we performed simulations in the $(\eta, \tau, \Delta\mu_s)$ -ensemble. For packing fractions η of hard discs that lie within the binodal curve, we can observe two-phase coexistence in the simulation box. The packing fractions of the coexisting phases can be obtained from the resulting density profiles of the hard discs. We also use the grand-canonical staged-insertion technique [23] together with the transition matrix MC method [24] to determine phase coexistence accurately for states close to the critical point of the solvent.

Mean-field expression for the Helmholtz free energy

Within a mean-field theory the Helmholtz free energy (per lattice site) of the incompressible ABC mixture can be decomposed as $F = F_C + F_{AB} + U_{BC}$, with (i) the pure-colloid contribution $F_C(\eta, T)$ for which we take the hard-disc free energy for the fluid phase from Ref. [25], and for the solid phase from [26] (ii) the mean-field free energy $F_{AB}(x, \eta, T)$ of the binary AB mixture in the free space in between the colloids (with fractions $1-x'$ and $x' \equiv x/(1-\eta)$ of A and B, respectively), and (iii) the average adsorption energy U_{BC} of the B solvent on the colloid surfaces. This yields, up to irrelevant constants,

$$F(\eta, T, x) = F_C(\eta, T) + \frac{2\epsilon x(1-x-\eta)}{(1-\eta)} + k_B T \left[x \ln \frac{x}{1-\eta} + (1-x-\eta) \ln \left(\frac{1-x-\eta}{1-\eta} \right) \right] - \frac{Z\alpha\epsilon}{v_c} \frac{x\eta}{1-\eta} \quad (2)$$

where $Z \simeq 2\pi R$ is the effective colloidal coordination number and where $v_c \simeq \pi R^2$ is the effective volume (area in 2D) of the colloid. The results of Fig. 5 are based on $Z\alpha = 32$ and $v_c = 1000$, which are not the same values used in our simulation studies. The purpose of using this mean field description is merely to understand the simulation phase diagrams qualitatively and to explore the existence of an underlying metastable lower G-L critical point.

* m.dijkstra1@uu.nl

- [1] Flöter, G. & Dietrich, S. Universal amplitudes and profiles for critical adsorption. *Z. Phys. B* **97**, 213–232 (1995).
- [2] Fisher, M. E. & de Gennes, P. G. Wall Phenomena in a critical binary mixture. *C. R. Acad. Sci. Paris B* **287**, 207–209 (1978).
- [3] Casimir, H. B. G. On the attraction between two perfectly conducting plates. *Kon. Ned. Akad. Wetensch. Proc.* **51**, 793 (1948).
- [4] Krech, M. *The Casimir Effect in Critical Systems* (World Scientific, Singapore, 1994).
- [5] Evans, R. & Stecki, J. Solvation force in two-dimensional Ising strips. *Phys. Rev. B* **49**, 8842–8851 (1994).
- [6] Hanke, A., Schlesener, F., Eisenriegler, E. & Dietrich, S. Critical Casimir forces between spherical particles in fluids. *Phys. Rev. Lett.* **81**, 1885–1888 (1998).
- [7] Krech, M. Fluctuation-induced forces in critical fluids. *J. Phys. Condens. Matter* **11**, R391 (1999).
- [8] Vasilyev, O., Gambassi, A., Maciolek, A. & Dietrich, S. Universal scaling functions of critical Casimir forces obtained by Monte Carlo simulations. *Phys. Rev. E* **79**, 041142 (2009).
- [9] Hertlein, C., Helden, L., Gambassi, A., Dietrich, S. & Bechinger, C. Direct measurement of critical Casimir forces. *Nature* **451**, 172–5 (2008).
- [10] Gambassi, A. *et al.* Critical Casimir effect in classical binary liquid mixtures. *Phys. Rev. E* **80**, 061143 (2009).
- [11] Mattos, T. G., Harnau, L. & Dietrich, S. Many-body effects for critical Casimir forces. *J. Chem. Phys.* **138**, 074704 (2013).
- [12] Mohry, T. F., Maciolek, A. & Dietrich, S. Phase behavior of colloidal suspensions with critical solvents in terms of effective interactions. *J. Chem. Phys.* **136**, 224902 (2012).
- [13] Bernard, E. P. & Krauth, W. Two-step melting in two dimensions: First-order liquid-hexatic transition. *Phys. Rev. Lett.* **107**, 155704 (2011).
- [14] Evans, R. Fluids adsorbed in narrow pores - phase-equilibria and structure. *J. Phys. Condens. Matter* **2**, 8989–9007 (1990).
- [15] Pandit, R., Schick, M. & Wortis, M. Systematics of multilayer adsorption phenomena on attractive substrates. *Phys. Rev. B* **26**, 5112 (1982).
- [16] Pieranski, P. Two-dimensional interfacial colloidal crystals. *Phys. Rev. Lett.* **45**, 569–572 (1980).
- [17] Drzewiński, A., Maciolek, A. & Evans, R. Influence of capillary condensation on the near-critical solvation force. *Phys. Rev. Lett.* **85**, 3079–82 (2000).
- [18] Okamoto, R. & Onuki, A. Casimir amplitudes and capillary condensation of near-critical fluids between parallel plates: renormalized local functional theory. *J. Chem. Phys.* **136**, 114704 (2012).
- [19] Bonn, D. *et al.* Direct observation of colloidal aggregation by critical Casimir forces. *Phys. Rev. Lett.* **103**, 156101 (2009).
- [20] Nguyen, V. D., Faber, S., Hu, Z., Wegdam, G. H. & Schall, P. Controlling colloidal phase transitions with critical Casimir forces. *Nat Commun* **4**, 1584 (2013).
- [21] Veatch, S. L. *et al.* Critical fluctuations in plasma membrane vesicles. *ACS Chemical Biology* **3**, 287–293 (2008).
- [22] Rabani, E., Reichman, D. R., Geissler, P. L. & Brus, L. E. Drying-mediated self-assembly of nanoparticles. *Nature* **426**, 271–274 (2003).
- [23] Ashton, D. J. & Wilding, N. B. Grand canonical simulation of phase behaviour in highly size-asymmetrical binary fluids. *Mol. Phys.* **109**, 999–1007 (2011).
- [24] Errington, J. R. Evaluating surface tension using grand canonical transition matrix Monte Carlo simulation and finite size scaling. *Phys. Rev. E* **67**, 012102 (2003).
- [25] Santos, A., López de Haro, M. & Bravo Yuste, S. An accurate and simple equation of state for hard disks. *J. Chem. Phys.* **103**, 4622 (1995).
- [26] Young, D. A. & Alder, B. J. Studies in molecular dynamics. XVII. Phase diagrams for "step" potentials in two and three dimensions. *J. Chem. Phys.* **70**, 473–481 (1979).

Acknowledgements: We thank N. Wilding, D. Ashton and A. Maciolek for stimulating discussions. J.R.E. and M.D. acknowledge financial support from a Nederlandse Organisatie voor Wetenschappelijk Onderzoek (NWO) VICI grant. N.T. and M.D. acknowledge financial support from an NWO-ECHO grant. J.R.E., N.T. and M.D. acknowledge a NWO-EW grant for computing time in the Dutch supercomputer Cartesius. R.E. acknowledges financial support from the Leverhulme Trust.

Author contributions: J.R.E. and M.D. initiated the simulation part of the project. N.T. and J.R.E. performed the simulations and were supervised by M.D.. S.B. and J.R.E. worked on the theory and were supervised by R.v.R.. J.R.E., N.T., S.B., R.E., R.v.R., and M.D. co-wrote the paper. All authors analyzed and discussed results.